Estimation of fatigue evolution of aluminum alloy plated with electroless Ni-Co-P by using electromagnetic impedance method

Katsuyuki Kinoshita

Department of Energy Conversion Science, Graduate School of Energy Science, Kyoto University, Yoshida-Honmachi, Sakyo-ku, Kyoto 606-8501, Japan

Abstract:

We have developed a method for detecting fatigue in aluminum alloys that is based on a applying a ferromagnetic electroless Ni-Co-P plating and then using an electromagnetic impedance (EMI) method to determine its permeability properties by measuring the high-frequency AC impedance of a coil sensor in the presence of a static magnetic field. The results obtained confirmed that this method can estimate the fatigue evolution of a specimen until the point at which the cumulative strain becomes saturated by using measurements obtained by the EMI method under tensile deformation and FEM analysis results.

Keywords:

Ni-Co-P plating; Aluminum alloy; Fatigue; Electromagnetic impedance method

1. Introduction

The evaluation of fatigue evolution is crucial in maintaining machines and structures; and to this end, various nondestructive testing methods such as the ultrasonic method, infrared thermography method and magnetic method have been developed. Among these, the magnetic

method (see, for example, Ref. [1]) has generally proven to be superior in that the equipment needed is simple and the measurements are easy to perform in an external environment. However, it can only be applied to ferromagnetic materials such as steel or nickel, and is therefore not applicable to light metals or non-metals.

Electroless plating is commonly used to improve the hardness and corrosion resistance of materials; for example, electroless nickel-phosphorus plating can increase the bending fatigue strength of 1050 aluminum alloy [2]. Ferromagnetic electroless Ni-Co-P films have also attracted attention as a thin-film magnetic recording medium [3], but as their hardness (~600 Hv) is comparable to that of Ni-P, an improvement in fatigue strength may also be expected. In addition, the presence of ferromagnetism makes possible an estimation of the progress of deterioration by measuring the magnetic properties of the Ni-Co-P film. In other words, electroless plating of an aluminum alloy with a Ni-Co-P film can potentially produce a multi-functional composite with high specific strength, and fatigue strength, combined with sensor functionality. In the past, fatigue sensors have been based on using grain growth and slip bands in plating under cyclic deformation [4], but there have been very few studies pertaining to using variations in the magnetic properties of a plating. Because the magnetic properties of a thin film such as Ni-Co-P plating are strongly influenced by the substrate, a special high-sensitivity device is required to measure them. A superconducting quantum interface device (SQUID) magnetometer can be used for this purpose, but unfortunately requires liquid helium cooling and is hard to use in the field.

In a previous study, we proposed using an electromagnetic impedance (EMI) method to estimate the magnetic properties of a ferromagnetic metal, which entailed measuring the high-frequency AC impedance of a coil sensor in the presence of an excited static magnetic field [5]. As this method employs the skin effect, it can be used to measure the magnetic properties of a ferromagnetic thin film or a ferromagnetic surface layer. In this way, we were able to estimate the

residual strain in an aluminum alloy with an electroless Ni-Co-P plating [6], along with the magnetic properties of the surface layer in SUS 304 steel [7]. The low- and high-cycle fatigue properties of electroless Ni-Co-P plated aluminum alloy were also measured using the EMI method, which found that the magnetic properties of the plating change with the cycle number [8], [9]. Although it was assumed at the time that this phenomenon was caused by the internal stress, this was simply because the stress and strain dependences of the plating's magnetic properties were not investigated.

The purpose of this study, therefore, was to identify the precise cause for the variation in the magnetic properties of an electroless Ni-Co-P plating with cycle number. To achieve this, the measurement system and results relating to impedance change caused by fatigue were first explained. Next, the impedance curves were measured under several tensile strains to evaluate the relationship between the magnetic properties of the plating and the tensile strain. Then finally, the relationship between impedance and the magnetic permeability vector was investigated through FEM analysis to ascertain the cause behind the plating's changing permeability properties.

2. Fatigue level measurement system

2.1 Out-of-plane−excited EMI method

The principle of measuring the magnetic properties of a plating using the EMI method can be explained as follows. As shown in Fig. 1, when an alternating current flows through a coil located above a test piece, eddy currents and an alternating magnetic field are induced in the surface of the test piece. The coil impedance is then determined from the lift-off distance, the shape and dimensions of the coil, and the magnetic permeability and electric resistivity of the test piece surface [10]. When a static magnetic field is applied to the test piece, the coil impedance also changes due to the change in the magnetic permeability of the ferromagnetic plating. Thus, if the

coil impedance is measured only during periods in which the magnetic field is held constant, then the magnetic field dependence of the permeability of the plating can be measured. Because the magnetic permeability of ferromagnetism is dependent on plastic deformation and stress, aspects of deterioration such as fatigue can be evaluated by using this method. This offers two distinct advantages: it can measure the permeability properties of a ferromagnetic thin film or ferromagnetic surface layer by using the skin effect, and it can measure the permeability properties in an arbitrary direction by changing the direction of the magnetic field. In this study, test pieces were excited perpendicular to their surface using a permanent magnet, and a pancake-type coil was used to measure the permeability properties in the out-of-plane direction. Since the excitation system was based on a permanent magnet, which unlike an electromagnet does not require a power source, it can be readily miniaturized for use in a system that is easy to use in the field.

2.2 Evaluation of impedance curves

The impedance generated in the presence of a magnetic field can be calculated by combining the theoretical formula for coil impedance with a magnetic model such as the Jiles−Atherton model [11]; however, it is impossible to derive an exact formula relating the impedance to the magnetic field as the magnetic model is nonlinear. It is therefore necessary to instead extract select values from a plot of impedance versus magnetic field to obtain any useable information about the deterioration. In this study, the impedance−magnetic-field curves were fitted to the exponential function given by Eq. (1), and the coefficients were used as the evaluation parameters. Eq. (1) can determine the saturation and nonlinearity characteristics of the impedance−magnetic-field curve obtained by the experiment. Moreover, it has the advantage that each of the coefficients strongly influences the shape of the curve as whole, much unlike the

coefficients of a polynomial.

$$\Delta Z(H) = \alpha \exp(-\beta H) + \gamma \quad (1)$$

The parameter α indicates the magnification of the exponential function, whereas β influences the shape of the curve. The parameter γ indicates the asymptotic value of the function and ΔZ is the relative change, given as $\Delta Z = (Z(H) - Z(0))/Z(0)$, in the presence of an external magnetic field H. Note that this ΔZ only permits evaluation of the magnetic permeability, as the permeability of ferromagnetism is more strongly dependent on the magnetic field than the electric resistivity is.

2.3 Dependence of cyclic deformation on impedance change

This section provides example measurements of the permeability properties of the plating under cyclic deformation. For this, fatigue tests were carried out at room temperature using a plane-bending fatigue testing machine at a frequency of 17 Hz and a stress ratio −1. Fig. 2 depicts the relationship between the ratio of the impedance change (ΔZ) and the cycle number (1×10^1, 1×10^5, and 4×10^5) for an applied stress of 83 MPa, in which we see that both the value of ΔZ and its slope decrease with increasing cycle number. Fig. 3 shows the relationship between the evaluation coefficient α and the fatigue level for two flat specimens, S1-1 and S1-2, each of which had a continuous radius between the grip ends (thickness 2 mm, radius 46 mm) and an average plating thickness of about 19 μm. The results obtained for β and γ show a tendency similar to that of α, in that an initial rapid decrease in value (stage 1) is followed by a more gradual decrease (stage 2), and then remains practically constant until the break point (stage 3) with increasing fatigue. Note, however, that there is a slight increase in α just before the point of rupture.

3. Experimental method

3.1 Specimens

The Ni-Co-P films were electrolessly plated onto 1050 aluminum alloy (H24) specimens; the size and shape of which are shown in Fig. 4. Before deposition, the surfaces of the test samples were subjected to mechanical polishing and buffing. The average thickness of each plating was 20 μm, and the composition of the bath and the operating conditions used are summarized in Table 1. The S-N curves obtained from bending fatigue tests of the 1050 aluminum alloy substrate and test pieces plated with Ni-Co-P are shown in Fig. 5. Note that the bending fatigue strength of those samples plated with Ni-Co-P film is 13−16% higher than that of the aluminum alloy substrate, thus confirming that Ni-Co-P plating produces a similar improvement in fatigue resistance as Ni-P plating.

3.2 Tensile strain dependence of impedance

Impedance measurement under tensile strain was carried out using the measurement system shown in Fig. 6. In this, a load is applied by a tensile testing machine (MicroTester, Instron Co. Ltd.), and the resulting tensile strain is measured using a 120-Ω single-unit strain gauge (type FLA, Tokyo Sokki Kenkyujo Co. Ltd.) with a quarter-bridge three-wire configuration and a dynamic strain amplifier (DPM-712B, Kyowa Dengyo Co.).

The impedance of a 60-turn pancake coil with an inner diameter of 5 mm and wire diameter of 100 μm was measured using an LCR meter (Hioki E.E, LCR HiTESTER 3532-50) at a lift-off distance of 0 mm. The excitation frequency was 5 MHz, and the excitation voltage was set at 1.0 V. The amplitude of the static magnetic field was controlled by moving a neodymium permanent magnet (diameter: 30 mm, thickness: 5 mm, maximum magnetic flux density: 190 mT)

perpendicular to the surface of the test sample.

4. FEM analysis

4.1 Analysis procedure

Finite-element simulations were carried out using commercial electromagnetic FEM software (Maxwell 3D, ANSYS, Inc.). To simulate the EMI method using FEM, two different analyses must be carried out: 1) a static magnetic field analysis to calculate the variation in the magnetic permeability that is created by the permanent magnet and 2) a harmonic magnetic field analysis to calculate the coil impedance. Since Maxwell3D does not include a function to translate the data in an element between static magnetic field and harmonic magnetic field analysis, we instead translated the data between analyses using blocks composed of a finite number of elements. A quarter-symmetry static magnetic field analysis model composed of a permanent magnet, Hall sensor, and test piece is shown in Fig. 7(a) and (b); and a quarter-symmetry harmonic magnetic field analysis model composed of an acrylic bobbin, coil, and test piece is shown in Fig. 8(a) and (b). In both instances, every copper wire was modeled and the plating of the test piece was divided into blocks of 0.5 mm × 0.5 mm × 0.019 mm, as shown in Fig. 7(b) and Fig. 8(b).

The FEM analysis was carried out as follows:

(a) Preprocess

1) Six models were created for the static magnetic field analysis of different distances between the permanent magnet and the test piece, h (= 5, 10, 15, 20, 25, and 30 mm).

2) Six models were also created for the harmonic magnetic field analysis of a scenario wherein the permanent magnet is replaced with the coil from static magnetic field analysis models.

(b) Static magnetic field analysis

1) The average element magnetic field vectors $\boldsymbol{H}^i_{\mathrm{ave}}$ in each block i were calculated according to the model.

2) The external magnetic field H_z in the thickness direction was calculated from the magnetic flux density in the Hall sensor model.

(c) Determination of the differential permeability

1) The value of f (H), which is a function of μ_{d} (where μ_{d} is the differential permeability), is obtained by measuring the initial magnetization curve and performing a spline interpolation. Next, the μ^i_{d} in each block of the model is obtained by assigning $\boldsymbol{H}^i_{\mathrm{ave}}$ to the function. The initial magnetization curve was measured by a SQUID magnetic flux meter (MPMS, Quantum Design, Inc.), which also measured the magnetization versus magnetic field curve in the longitudinal direction.

(d) Harmonic magnetic field analysis

1) The value of $\boldsymbol{\mu}^i_{\mathrm{dr}}$ was first set to the material parameter of the elements in each block according to the model (where μ_{dr} is the differential relative permeability).

2) The resistance R and inductance L of the coil were then calculated using Eq. (2).

$$R = \frac{\int J \cdot J^* dV}{\sigma I_{\mathrm{peak}}^2},\ L = \frac{\int \boldsymbol{B} \cdot \boldsymbol{H} dV}{I_{\mathrm{peak}}^2} \tag{2}$$

where J is the current density, σ is the electric conductivity, I_{peak} is the peak current flow in the wire, $\boldsymbol{B}$ is the magnetic flux density vector, $\boldsymbol{H}$ is the magnetic field vector, and * is the complex conjugation operator.

(e) Constructing the impedance curve

1) The value of Z was calculated by assigning the values for R and L obtained using the model to the equivalent circuit equation for coil impedance (Eq. (3)). The capacitance C was determined

by trial and error to fall between the experimental and FEM results for free-space impedance.

$$Z = \frac{R}{(1-\omega^2 LC)^2 + (\omega RC)^2} + j\omega \frac{(L - \omega^2 L^2 C - R^2 C)}{(1-\omega^2 LC)^2 + (\omega RC)^2} \quad (3)$$

where ω is the angular frequency of the current and j is the complex number.

2) Finally, a Z versus H_z curve was created from the results of all the models.

4.2 Magnetic flux density versus magnetic field curve

The curves shown in Fig. 9 were used to represent the magnetic flux density B versus magnetic field H for the static magnetic field analysis. Curve A is a B−H curve calculated from the M−H curve that was obtained by the SQUID magnetic flux meter. Curve B was also calculated from the M−H curve by multiplying it by 0.4 to simulate a B−H curve for the hard magnetization direction. The other material constants used in the FEM analysis are provided in Table 2.

5. Results

5.1 Relationship between the ratio of impedance change and tensile strain

Fig. 10 shows ΔZ versus the magnetic field curve under several tensile strains, while Fig. 11 shows the evaluation coefficient α versus the tensile strain curve for the two specimens S2-1 and S2-2. For reference, the stress−strain curve is also given in Fig. 11. These results demonstrate that the maximum variance of ΔZ decreases with increasing tensile strain, and exhibits a similar tendency to that for the number of cycles. Moreover, α decreases significantly at tensile stresses ≤ 50 MPa (the elastic limit), but decreases almost linearly when the tensile stresses is > 50 MPa and begins to generate a residual strain. Because the test pieces broke at a tensile strain of about 3500 με, the permeability of the Ni-Co-P plating evidently changes with increasing tensile strain

provided the tensile strain does not exceed the fracture strain of the Al substrate.

5.2 Relationship between the ratio of impedance change and the permeability vector

To investigate the effects of the permeability vector on the coil impedance, the B–H curves A and B shown in Fig. 9 were applied with an arbitrary axial direction for each of the analysis conditions shown in Table 3. Condition 1 is that the B–H curves for all directions correspond to curve A. Condition 2 is that the B–H curves for the width and thickness directions correspond to curve A, whereas that for the length direction corresponds to curve B. Condition 3 is that the B–H curves for the in-plane direction correspond to curve A and that for the thickness direction corresponds to curve B. Fig. 12 shows the relationship between the ratio of impedance change and the magnetic field, and also the relationships between the permeabilities of the plating in the length and thickness directions and the magnetic field under Condition 1. Note that in this instance, the permeability in each direction is an average taken from each direction of the Ni-Co-P blocks within a 3 mm × 3 mm area under the coil. This calculated data for the change in impedance with the magnetic field is similar to experimentally obtained results; however, the permeability in the thickness direction (the excitation direction) changes almost imperceptibly at magnetic fields ≤ 20 kA/m. On the other hand, the permeability in the length direction (the tensile strain direction) changes quite significantly with magnetic fields of ≤ 20 kA/m and corresponds to the ΔZ curve. This suggests that the change in the impedance of the pancake coil induced by excitation in the thickness direction depends on the permeability in the in-plane direction rather than the thickness direction. This is further evidence by the relationships between ΔZ and the magnetic field under Condition 1, Condition 2, and Condition 3 that are shown in Fig. 13. These show that when the longitudinal direction is the hard magnetization direction, as is the case under

Condition 2, the maximum variation in ΔZ is lower than under Condition 1. Moreover, when the thickness direction is the hard magnetization direction, as it is under Condition 3, the shape of the $\Delta Z-H$ curve is almost identical to that under Condition 1. The reasons for this are as follows. Firstly, the fact that the Ni-Co-P plating is a film means that the thickness direction corresponds to the hard magnetization direction, as determined by the shape demagnetizing effect. Furthermore, because the magnetic field induced by the pancake coil creates a loop, as shown in Fig. 1, the magnetic flux density through the coil is affected by not only the permeability in the *z* direction, but also that in the *x* and *y* directions.

6. Discussion

The mechanism by which the impedance curve is changed by cyclic deformation can be explained by first considering its dependence on the in-plane direction that is evident from the analysis results in Section 5.2. We also need to consider the results of Section 5.1, which show that the α value corresponding to the maximum variation in permeability decreases with increasing tensile strain, and that the tensile direction is the magnetic hard axis of the Ni-Co-P plating. Taken together, this means that residual strain accumulates in the in-plane direction of the substrate during the cyclic loading, and an internal stress is therefore generated in the Ni-Co-P plating along this same direction. The permeability in the in-plane direction of the Ni-Co-P plating is subsequently changed by this internal stress, which in turn alters the impedance of the pancake coil.

The change in the evaluation coefficient α with repeated cycles of deformation is related to the fact that the strain amplitude in metals such as Al and Cu generally increases quite gradually at low-cycle numbers, and then remains constant in stress-controlled low-cycle fatigue tests [13]. It

is therefore not surprising that the residual strain also increases rapidly at low-cycle numbers, and then saturates with increasing cycle number. The rapid decrease in α in stage 1 can be explained by the fact that this represents the cycle number range in which the tensile residual strain increases rapidly; and as shown in Fig. 11, equates to a tensile strain region of < 1000 $\mu\varepsilon$ in which α is known to change substantially. Similarly, the gradual decrease in α in stage 2 is due to this representing a residual tensile strain of ≥ 1000 $\mu\varepsilon$. The lack of change in α in stage 3 could be the result of one of two: the residual strain of the substrate saturates with cycle number, and the permeability of the Ni-Co-P plating does not change with stress as its deformation is greater than the saturation magnetostriction. However, in this instance it is not possible for the latter reason to be correct due to the fact that α changes at the strain level at which the substrate breaks, as shown in Fig. 11.

This increase α that is observed just before fracture requires both a decrease in the residual strain in the aluminum alloy substrate and an increase in the permeability of the Ni-Co-P plating. A similar increase in stress amplitude just before low-cycle fatigue fracture has previously been observed in Al-Mg-Si aluminum alloy [14], which suggests the possibility that the increase of α at the end of stage 3 corresponds to a decrease in the residual strain of the substrate. The lack of sufficient accuracy in the measurement of the residual strain just before fracture makes it impossible to verify this connection at present; however, if this is indeed the case then it could provide a means of predicting of the rupture life.

7. Conclusion

Through experimental and FEM analysis of problems associated with developing a system for estimating the fatigue level of aluminum alloy using electroless Ni-Co-P plating and the EMI

method, the following conclusions have been made:

(1) Measurements of the impedance under several tensile strains identified that the relationship between the evaluation coefficient and the tensile strain corresponds to the relationship between the evaluation coefficient and the number of cycles.

(2) FEM analysis of the relationship between impedance and the magnetic permeability vector found that the change in the impedance of the pancake coil is dependent on the permeability in the in-plane direction when excitation is in the thickness direction.

(3) The change in impedance with an increasing number of cycles is caused by magnetic permeability in the in-plane direction of the Ni-Co-P plating, which changes due to internal stress caused by the accumulation of residual strain in the substrate.

(4) The three steps in the evolution of the ratio of impedance change ΔZ with an increasing number of cycles can be explained by the relationship between the residual strain of the substrate and the number of cycles, and the dependence of the plating permeability on tensile strain.

(5) The proposed method can currently be used to evaluate the fatigue level up to saturation of residual strain in the substrate saturates, and has the potential to be applied in the future to predicting the rupture time.

Acknowledgments

We would like to thank Meltex Co. for their assistance with the plating solution sample used in this study. This work was partially carried out using facilities of the Research Center for Low Temperature and Materials Sciences, Kyoto University. The authors would also like to express their appreciation to the former graduate students of Yamaguchi University: Mr. Hirama Seiichi, Mr. Sugai Koichiro, Mr. Otuji Seishiro and Mr. Fujita Yohei for their help in creating the

experimental equipment and in the performance of the experiments.

References

[1] Stevens KJ. Stress dependence of ferromagnetic hysteresis loops for two grades of steel. NDT E Int 2000;33(2):111−121.

[2] Tagami M, Aso S, Goto S, Koike K. Effect of electroless Ni-P plating on the fatigue strength of aluminum. Light metal 1993;46(5):281−284. (in Japanese)

[3] Kim D-H, Aoki K, Takano O. Soft magnetic films by electroless Ni-Co-P plating. J Electrochem Soc 1995;142(11):3763−3767.

[4] Ono Y, Kitaoka S. Cyclic stress measurement method using grain size and occurrence rate of grown grains in electrodeposited copper foil. Strain 2011;47(2):154−161.

[5] Kinoshita K. Stress measurement under plastic deformation using the electromagnetic AC impedance wave method. J. Mag. Soc. Jpn. 2005;29:1004−1009. (in Japanese)

[6] Kinoshita K, Fujita Y. Development of magnetic fatigue sensing technology to aluminum alloy bay using ferromagnetic plating. Book of Abstracts of the 12th Joint MMM/Intermag Conference, Chicago January 2013. FX-15.

[7] Kinoshita K, Hasegawa Y, Matsumoto E. Non-destructive method for evaluation of deterioration of austenitic stainless steel using initial magnetic phase. International Journal of AEM 2012; 39:375–380.

[8] Hirama S, Kaminishi K, Kinoshita K. Development of magnetic fatigue sensing technology to aluminum alloy bay using ferromagnetic plating. Proc. of Jpn. Soc. Mech. Eng. 47th Tyugoku-shikoku. Branch Conf., March 2009. 35–36. (in Japanese)

[9] Otsuji S, Kinoshita K, Kaminishi K. Estimation of breaking point of aluminum alloy to high cycle fatigue tests using ferromagnetic deposit and electromagnetic AC impedance method, Proc.

MAGDA Conference, Sapporo November 2010, 555–558. (in Japanese)

[10] Dodd CV, Deeds WE. Analytical solutions to eddy-current probe-coil problems. J. Appl. Phys. 1968;39(6):2829–2838.

[11] Jiles DC, Thoelke JB, Devine MK. Numerical determination of hysteresis parameters for the modeling of magnetic properties using the theory of ferromagnetic hysteresis. IEEE Trans. Mag. 1992;28(1):27−35.

[12] Gao Y. The influence of cobalt on the corrosion resistance and electromagnetic shielding of electroless Ni-Co-P deposits on Al substrate. Applied Surface Science 2007;253:9470–9475.

[13] Polák J, Klesnil M, Lukáš P. High cycle plastic stress−strain response of metals. Mater. Sci. Eng. 1974;15:231–237.

[14] Borrego LP, Abreu LM, Costa JM, Ferreira JM. Analysis of low cycle fatigue in AlMgSi aluminium alloys. Engineering Failure Analysis 2004;11:715–725.

Figure captions

Fig. 1. Schematic showing the principles of electromagnetic impedance method.

Fig. 2. Relationship between the ratio of impedance change and the external magnetic field for different numbers of cycles.

Fig. 3. Relationship between the scale factor α and the fatigue level.

Fig. 4. Dimensions of the specimens used.

Fig. 5. S-N curves for A1050 alloy with and without an electroless Ni-Co-P plating.

Fig. 6. Schematic of the experimental setup used for measuring the impedance of tensile test samples.

Fig. 7. FEM analysis model for calculating the magnetic field of blocks excited by a permanent magnet.

Fig. 8. FEM analysis model for calculating the impedance of a coil.

Fig. 9. Relationship between magnetic flux density and magnetic field for calculating the influence of the permeability vector.

Fig. 10. Relationship between the ratio of the impedance change and the external magnetic field, as obtained experimentally at different tensile strains.

Fig. 11. Relationship between the scale factor α and the external magnetic field, as obtained experimentally at different tensile strains.

Fig. 12. Relationships of the external magnetic field to the impedance change (shown by filled circles), magnetic permeability in the *x* direction (shown by open triangles), and magnetic permeability in the *z* direction (shown by open squares).

Fig. 13. Plot of impedance change versus external magnetic field for Condition 1, Condition 2, and Condition 3.

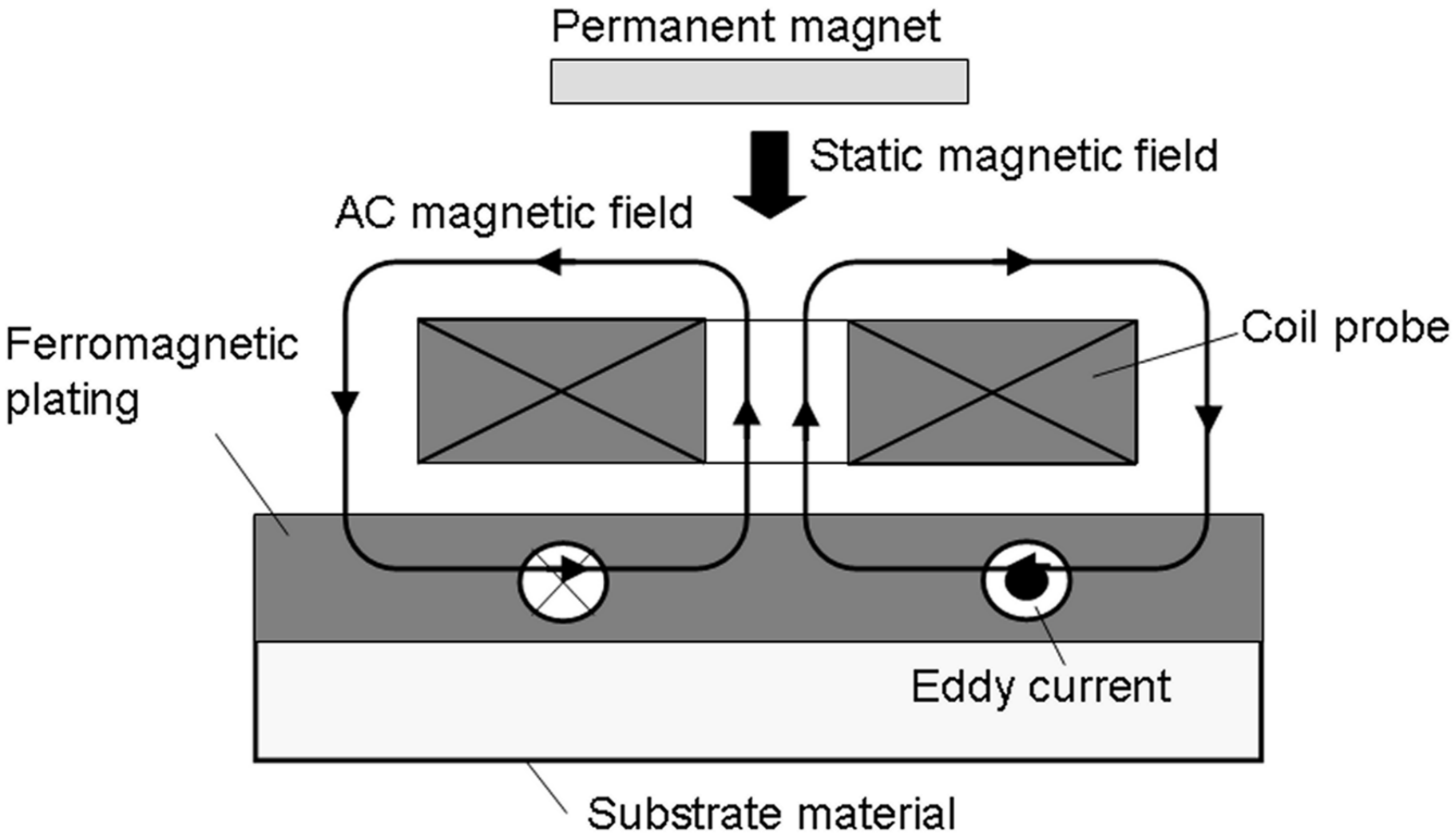
Permanent magnet
Static magnetic field
AC magnetic field
Ferromagnetic plating
Coil probe
Eddy current
Substrate material

Fig. 1

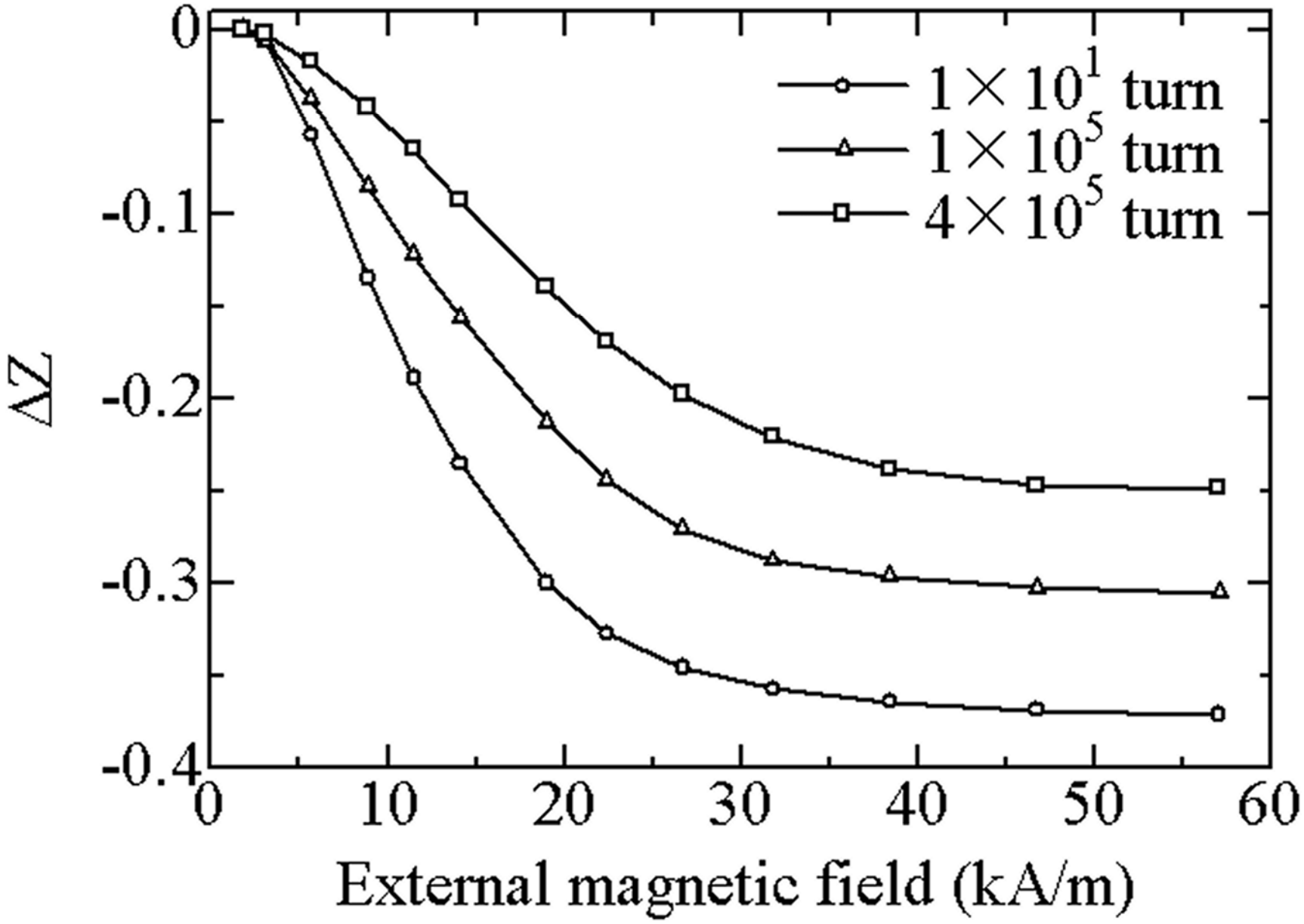
0
-0.1
-0.2
-0.3
-0.4
ΔZ
0
10
20
30
40
50
60
External magnetic field (kA/m)
1×10^1 turn
1×10^5 turn
4×10^5 turn

Fig. 2

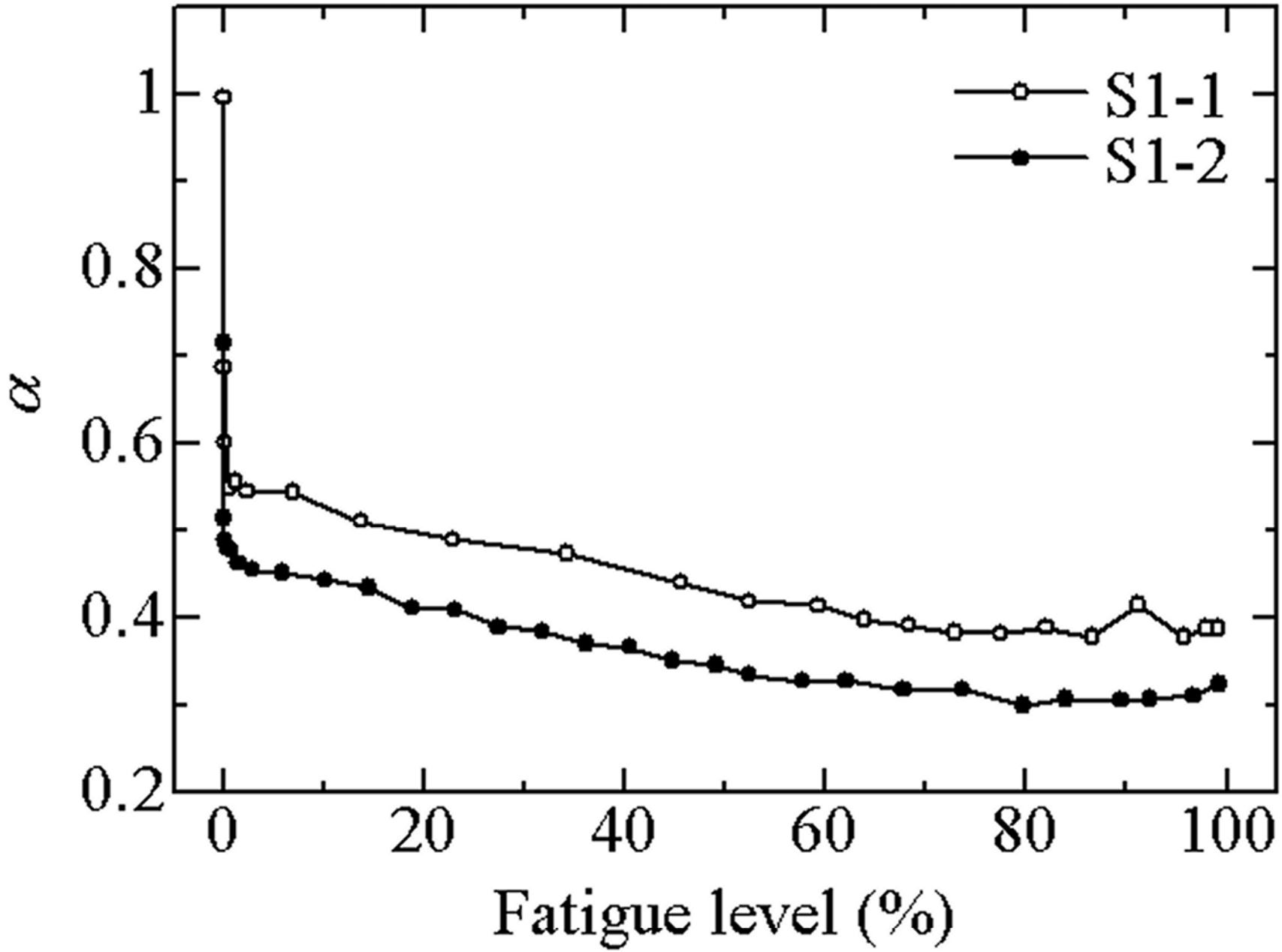

Fig. 3

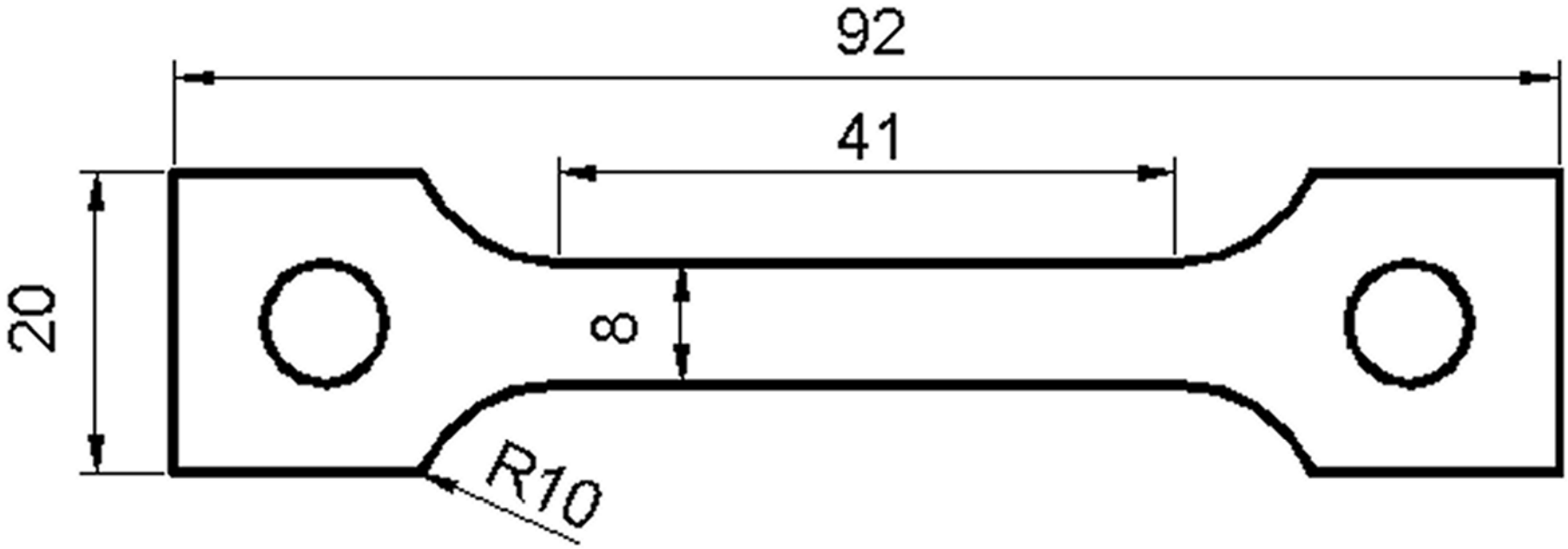

Fig. 4

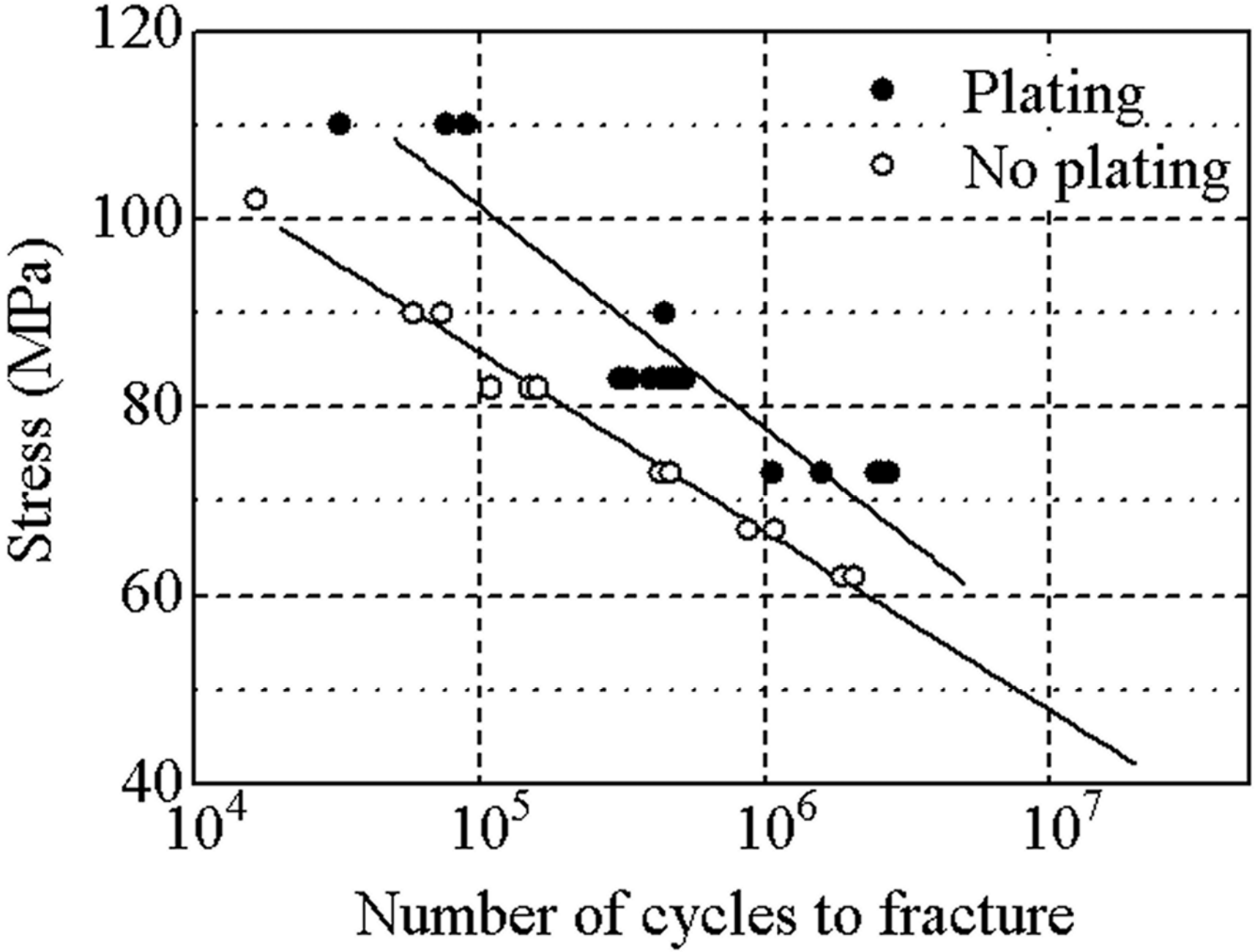
120
100
80
60
40
Stress (MPa)
Plating
No plating
10^4
10^5
10^6
10^7
Number of cycles to fracture

Fig. 5

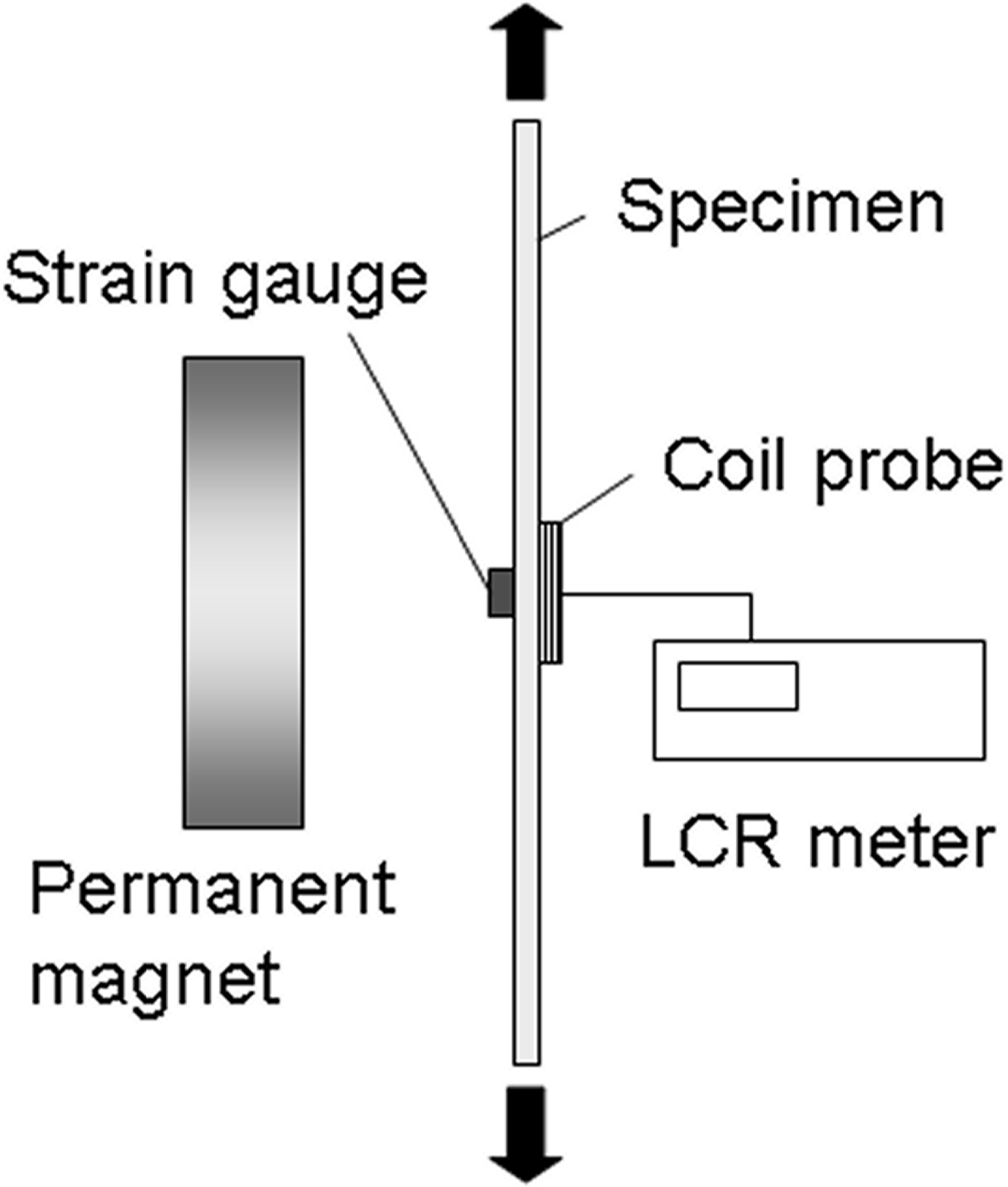
Specimen
Strain gauge
Coil probe
LCR meter
Permanent magnet

Fig. 6

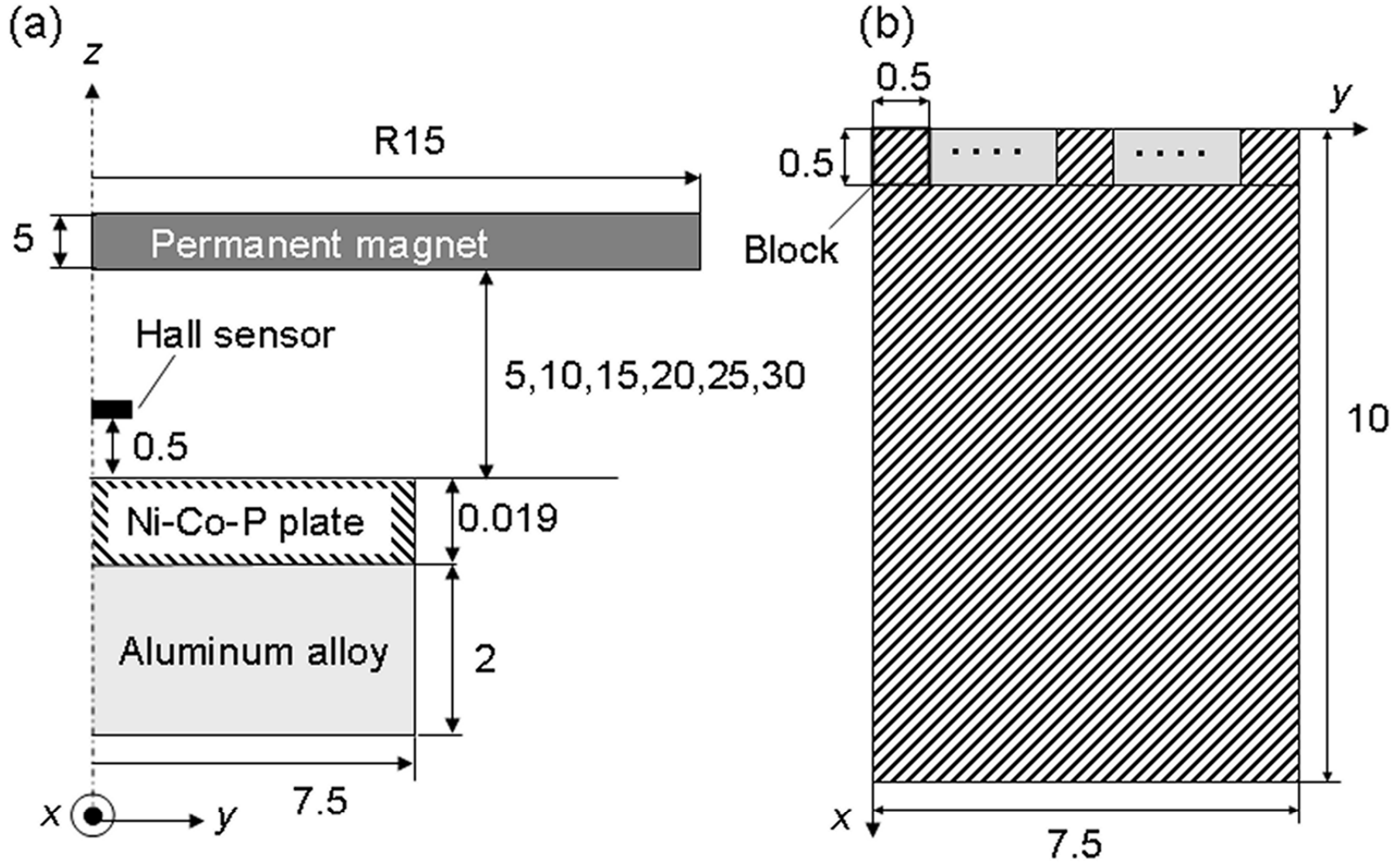
(a)
z
R15
5
Permanent magnet
Hall sensor
5,10,15,20,25,30
0.5
Ni-Co-P plate
0.019
Aluminum alloy
2
7.5
x
y
(b)
0.5
y
0.5
Block
10
x
7.5

Fig. 7

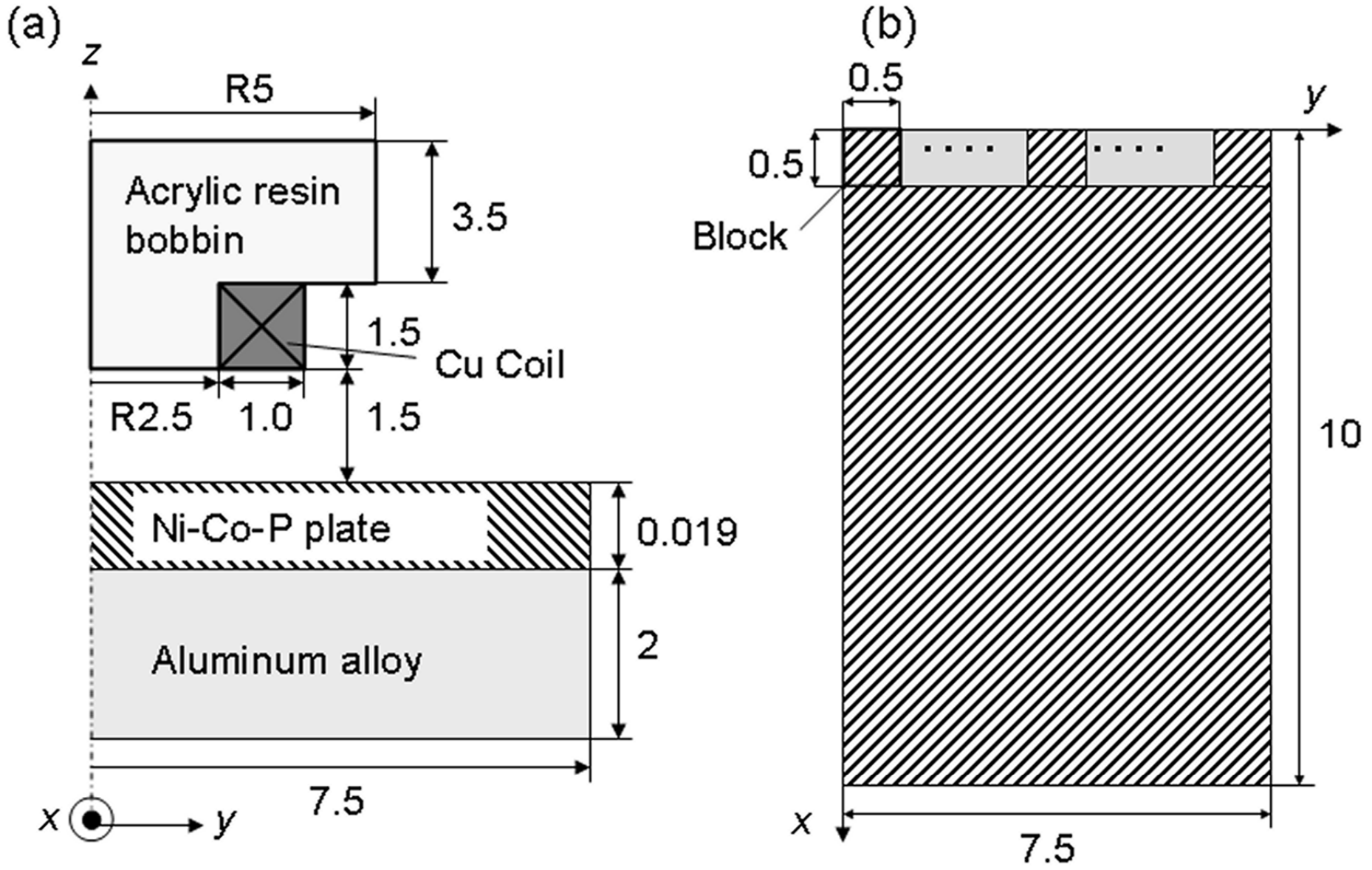
(a)
z
R5
Acrylic resin
bobbin
3.5
1.5
Cu Coil
R2.5
1.0
1.5
Ni-Co-P plate
0.019
Aluminum alloy
2
7.5
x
y
(b)
0.5
y
0.5
Block
10
x
7.5

Fig. 8

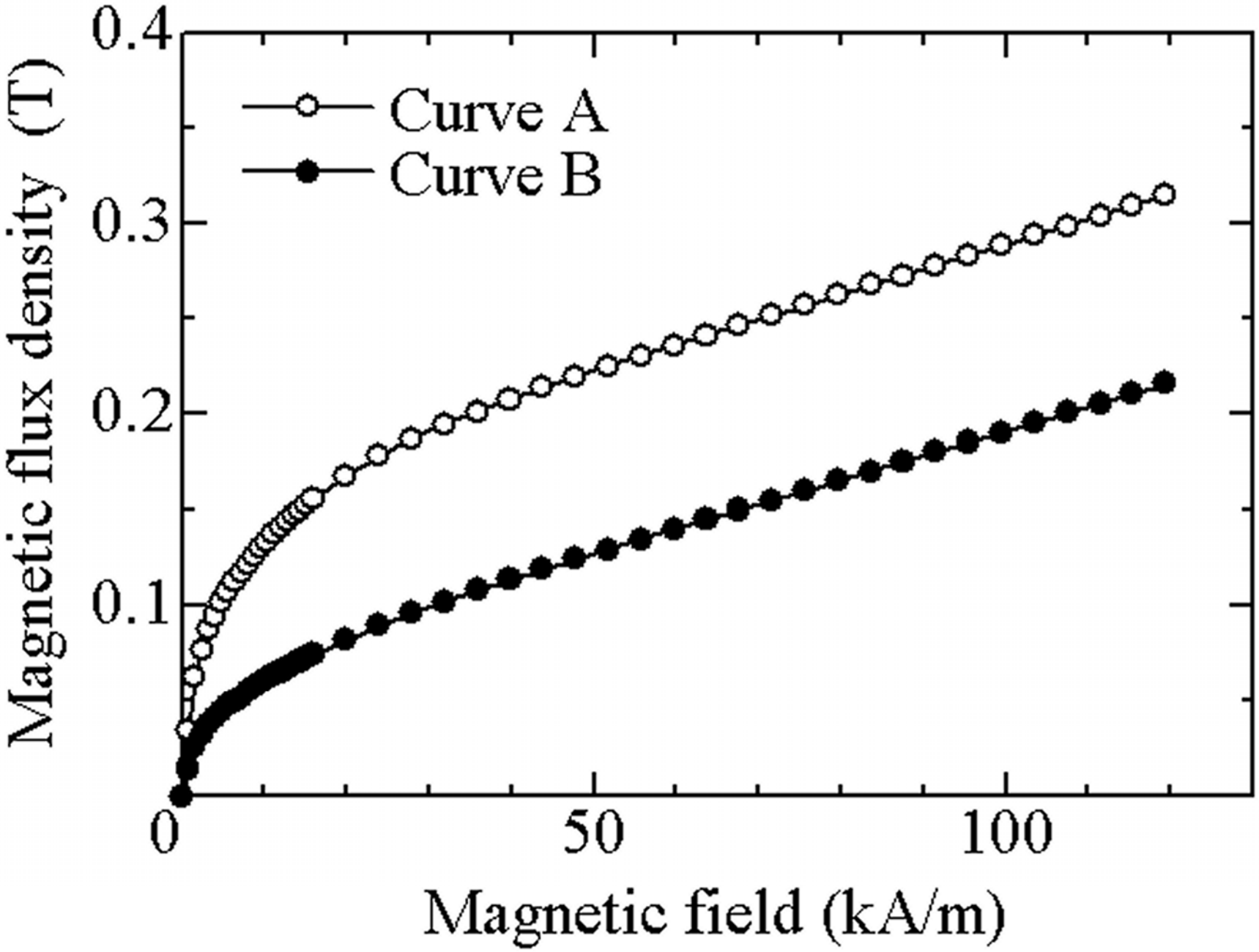
Curve A
Curve B
Magnetic flux density (T)
0.4
0.3
0.2
0.1
0
50
100
Magnetic field (kA/m)

Fig. 9

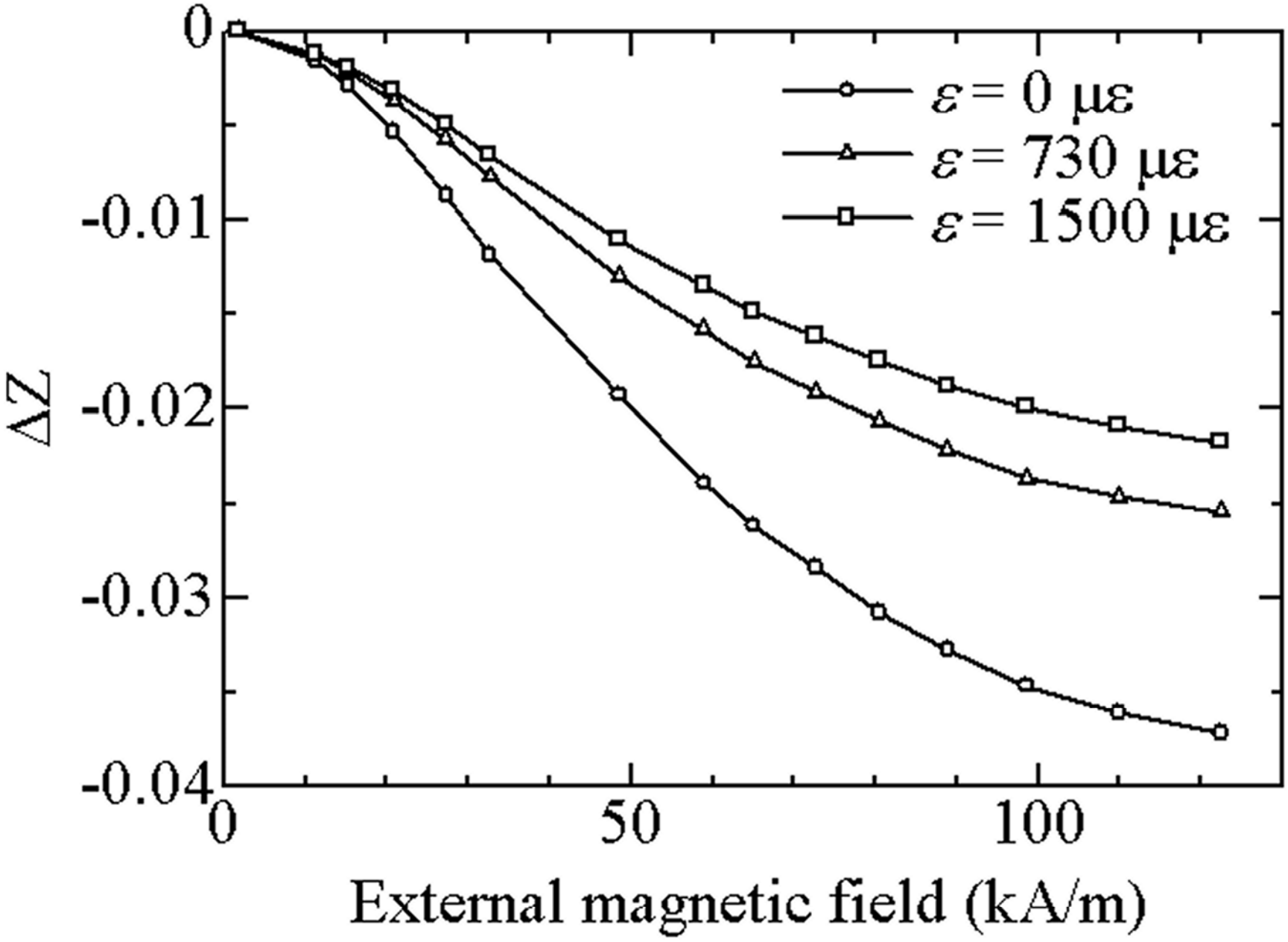
0
-0.01
-0.02
-0.03
-0.04
ΔZ
0
50
100
External magnetic field (kA/m)
ε = 0 με
ε = 730 με
ε = 1500 με

Fig. 10

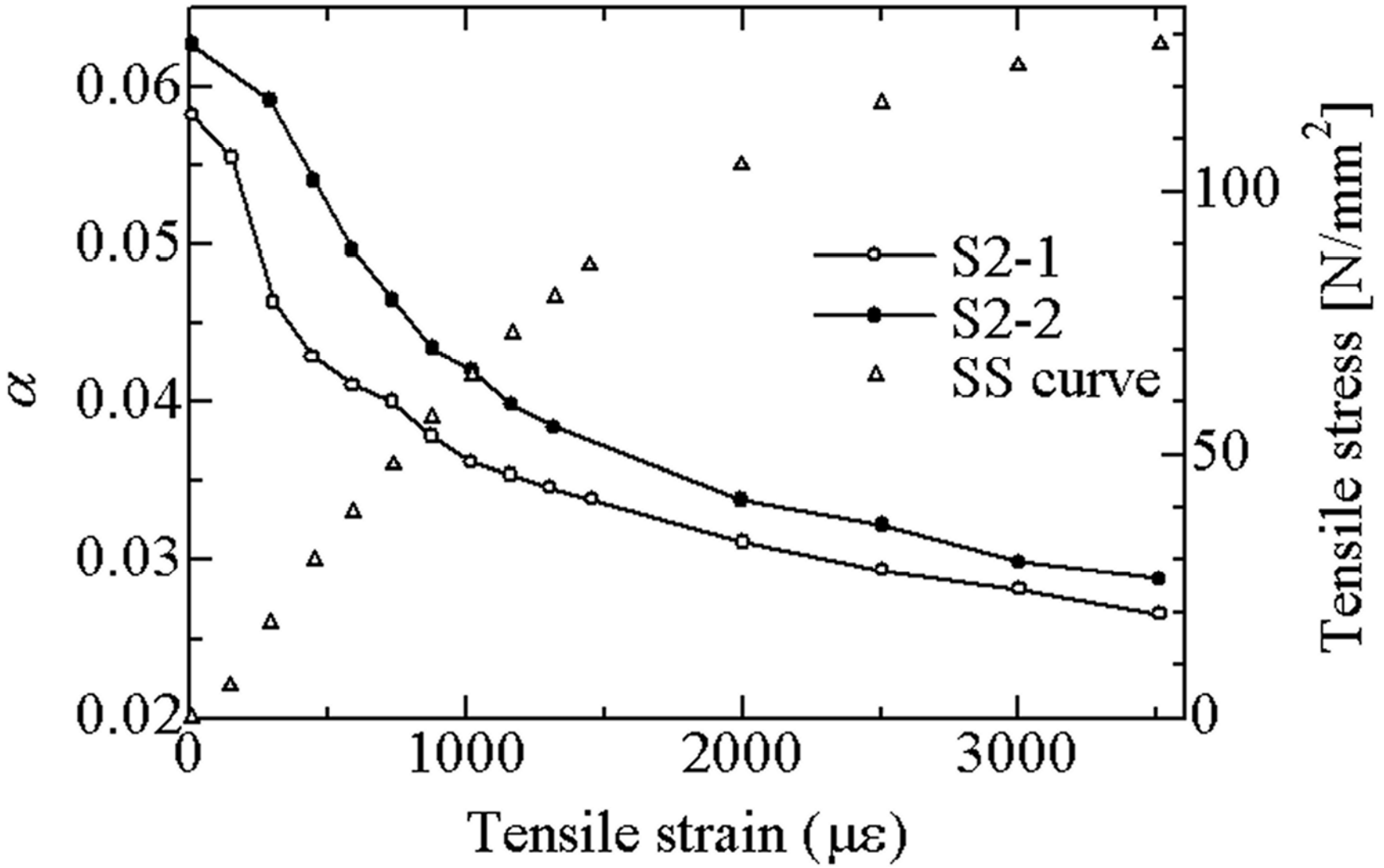
0.06
0.05
0.04
0.03
0.02
α
0
1000
2000
3000
Tensile strain (με)
100
50
0
Tensile stress [N/mm²]
S2-1
S2-2
SS curve

Fig. 11

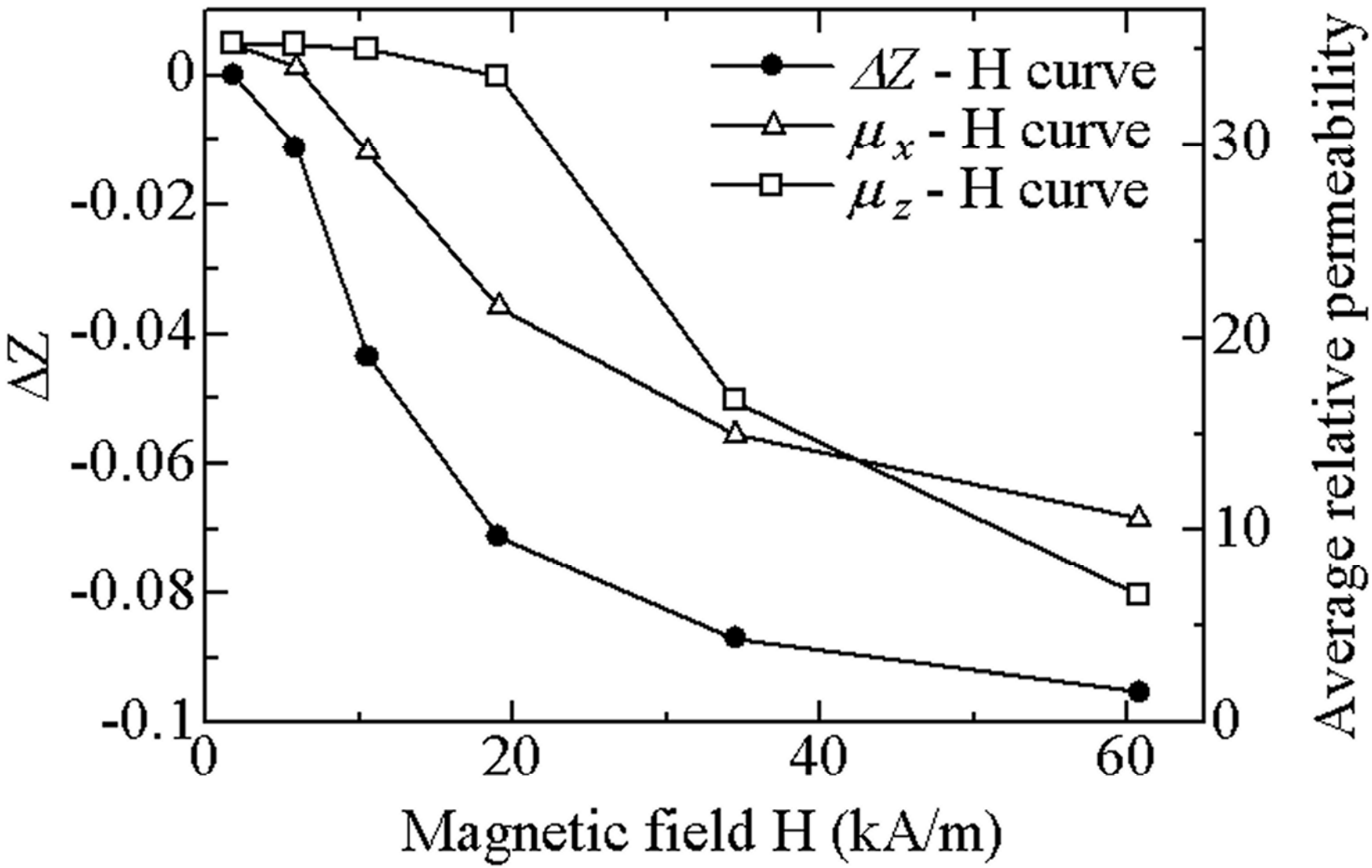
ΔZ - H curve
μx - H curve
μz - H curve
ΔZ
Average relative permeability
Magnetic field H (kA/m)
0
-0.02
-0.04
-0.06
-0.08
-0.1
0
20
40
60
30
20
10
0

Fig. 12

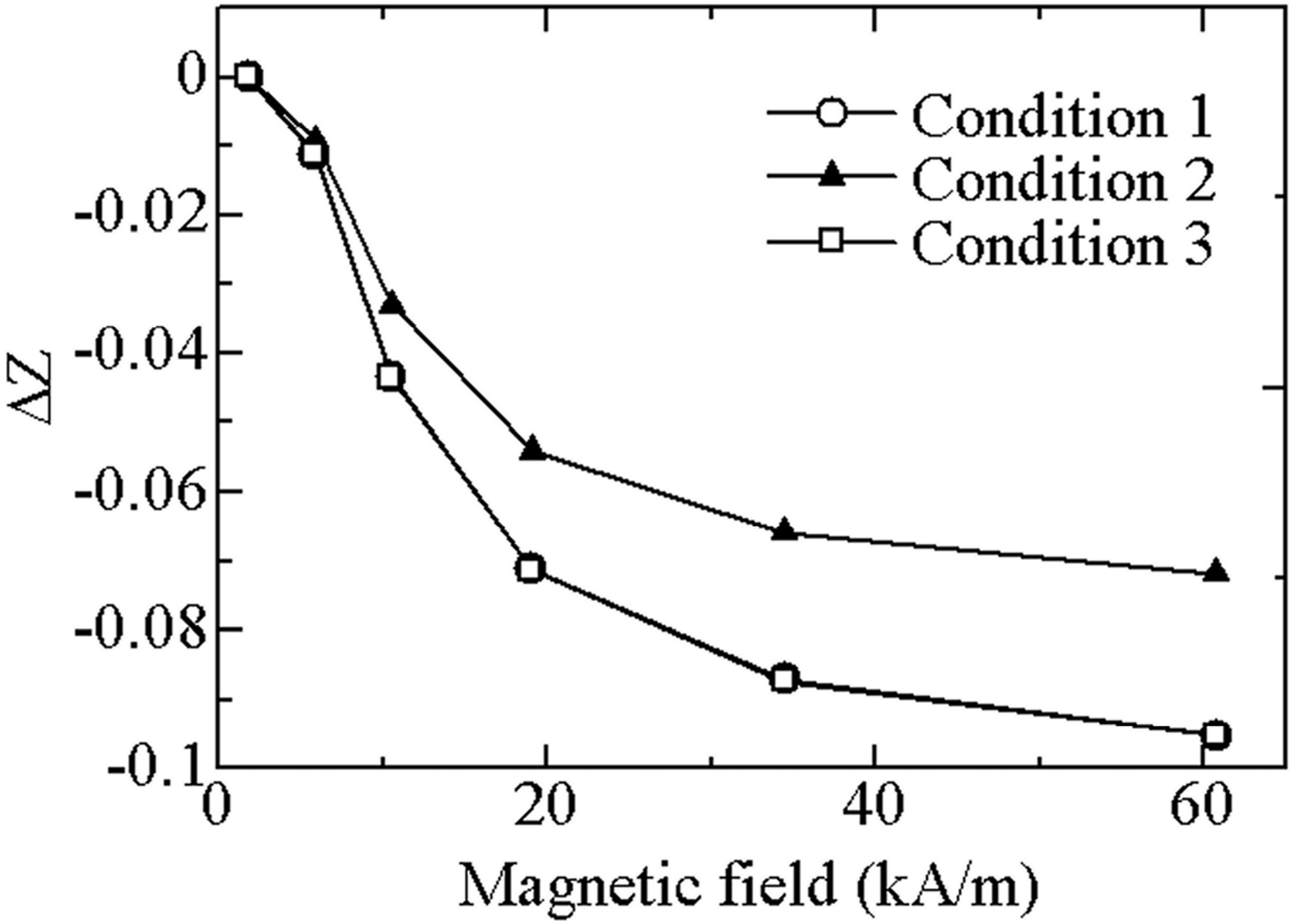
0
-0.02
-0.04
-0.06
-0.08
-0.1
ΔZ
0
20
40
60
Magnetic field (kA/m)
Condition 1
Condition 2
Condition 3

Fig. 13

Table 1
Bath compositions and plating conditions

$NiSo_4 \cdot 6H_2O$	0.08 mol/L
$CoSo_4 \cdot 7H_2O$	0.05 mol/L
$NaPH_2O2 \cdot H_2O$	0.33 mol/L
complexing agent	0.4 – 0.6 mol/L
stabilizer	micro amount
pH	8.0
bath temperature	363 K

Table 2
Material constants used for FEM

Material	Material properties		
	Relative permeability	Relative permitivity	Bulk conductivty (S/m)
Ni-Co-P	1	1	925925.9[12]
Alminum alloy	1.000021	1	38000000
Copper	0.999991	1	58000000
Acrylic resin	1	3.19	0
Air	1	1	0

Table 3
Relationships between magnetic flux density vector and magnetic field vector for each condition.

Condition	B_x-H_x curve	B_y-H_y curve	B_z-H_z curve
1	A	A	A
2	B	A	A
3	A	A	B